# Energy dependence of the total cross section for the $^{11}$Li + $^{28}$Si reaction

Yu. E. Penionzhkevich,[1,2,*] Yu. G. Sobolev,[1] V. V. Samarin,[1,3] M. A. Naumenko,[1] N. A. Lashmanov,[1] V. A. Maslov,[1] I. Siváček,[1,4] and S. S. Stukalov[1]

[1]*Flerov Laboratory of Nuclear Reactions, Joint Institute for Nuclear Research, Dubna 141980, Russia*
[2]*Department of Experimental Methods in Nuclear Physics, National Research Nuclear University, Moscow 115409, Russia*
[3]*Department of Nuclear Physics, Dubna State University, Dubna 141982, Russia*
[4]*Department of Nuclear Reactions, Nuclear Physics Institute of the Czech Academy of Sciences, Řež 25068, Czech Republic*

(Received 11 August 2018; revised manuscript received 2 November 2018; published 10 January 2019)

In this paper the results of measurements of the total cross sections for the $^{11}$Li + $^{28}$Si reaction in the beam energy range 7$A$–25$A$ MeV are presented. The experimental cross sections were obtained by registration of the prompt gamma and neutron radiation accompanying the interaction of $^{11}$Li nuclei with $^{28}$Si nuclei. The total cross sections for the $^{11}$Li + $^{28}$Si reaction are calculated based on a numerical solution of the time-dependent Schrödinger equation for the external weakly bound neutrons of the projectile nucleus $^{11}$Li. The calculated total reaction cross sections are in good agreement with the experimental data.

DOI: 10.1103/PhysRevC.99.014609

## I. INTRODUCTION

The study of nuclear reactions involving neutron-rich weakly bound nuclei makes it possible to obtain information on the structure of the investigated nuclei (clusters, neutron halo, etc.) and its manifestation in reactions [1]. Reactions with Li isotopes are of considerable interest from several points of view. Nuclei $^{6-11}$Li with the ratio of the number of neutrons to the number of protons varying from 1 to 2.67 and, therefore, with a significantly different structure provide a unique opportunity for testing various microscopic models. One of the criteria for the limits of applicability and the degree of accuracy of theoretical models is the quantitative agreement between the values of the calculated and the experimentally measured total cross sections of nuclear reactions.

The results of experiments on measuring total cross sections $\sigma_R(E)$ for the $^{9}$Li + $^{28}$Si reaction as a function of the beam energy in the range $E = 5A - 50A$ MeV performed by us earlier [2] showed that for the $^{9}$Li + $^{28}$Si reaction in the energy range $E = 10A - 20A$ MeV the values of the total cross section are much larger than those for the $^{7}$Li + $^{28}$Si reaction [3], which was not explained by the theoretical models existing at the time. In [2], it was assumed that the reason for the observed behavior was related to the properties of the shell of weakly bound external neutrons and its evolution in the process of collision with the target nucleus. In the $^{11}$Li nucleus, the external neutrons are even more weakly bound, which determines large interest in studying reactions with this nucleus. In particular, in Refs. [4,5] it was shown experimentally that the total cross sections for reactions involving weakly bound $^{6}$He and $^{11}$Li nuclei can be represented in the form $\sigma_R(^{6}\mathrm{He}) \approx \sigma_R(^{4}\mathrm{He}) + \sigma_{-2n}(^{6}\mathrm{He})$ and $\sigma_R(^{11}\mathrm{Li}) \approx \sigma_R(^{9}\mathrm{Li}) + \sigma_{-2n}(^{11}\mathrm{Li})$, respectively. When the nuclei with low neutron separation energy break up, a significant fraction of neutrons fly into the forward angles. In [6], differential cross sections for neutron emission in reactions of $^{11}$Li with Au, Ni, Be targets at the beam energy 29$A$ MeV were measured. It was shown that the emission of neutrons is strongly anisotropic with a maximum yield in a narrow range of forward angles.

This paper is devoted to measurements and calculations of the total cross sections for the $^{11}$Li + $^{28}$Si reaction. Most experiments using the method of direct measurement of total cross sections of nuclear reactions can be divided into two groups: the beam transmission methods and the beam attenuation methods, first used in [7] and [8], respectively.

In the present work, to study the $^{11}$Li + $^{28}$Si reaction the transmission method was used. Section II describes the experimental setup and the experimental procedure. Section III is devoted to determining the efficiency of detection of gamma quanta of different multiplicities by the spectrometer used. Section IV describes the procedure of analysis of experimental data for reactions with the $^{6}$He and $^{9,11}$Li nuclei taking into account anisotropy of neutron emission from weakly bound projectile nuclei. The measured total cross section for the reaction with the $^{6}$He nucleus was normalized to data obtained earlier in other studies. The dependence of the corrections from neutron emission anisotropy on the separation energy of one and two external neutrons of the $^{6}$He nucleus was determined; the correction for $^{11}$Li was determined by linear extrapolation. Section V describes the shell model for the $^{9,11}$Li nuclei. Section VI presents calculations of the total cross sections for the $^{11}$Li + $^{28}$Si reaction based on the model of the $^{11}$Li nucleus as a system of a $^{9}$Li core and two neutrons and description of the evolution of the external neutron wave function using a numerical solution of the time-dependent Schrödinger equation. Section VII is devoted to the comparison of the obtained experimental data with theoretical predictions.

*pyuer@jinr.ru

 

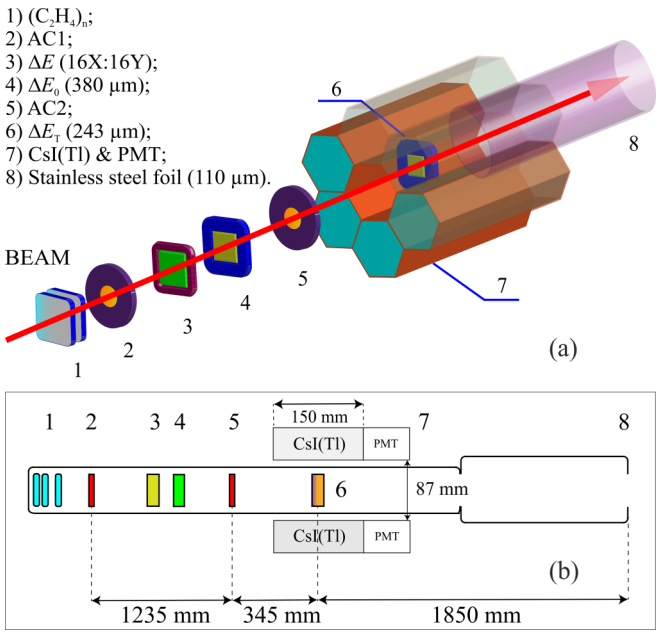


FIG. 1. Three-dimensional scheme of the experimental setup (a) and its section with the dimensions (b): (1) polyethylene plates for reducing the energy of the beam particles; (2) scintillation detector AC1; (3) position-sensitive Si detector $\Delta E$ (16X:16Y); (4) start $\Delta E_0$ Si detector; (5) scintillation detector AC2; (6) target $\Delta E_T$ Si PIN detector; (7) CsI(Tl) scintillation $\gamma$ spectrometer; (8) window for the output of the beam (stainless steel foil).

## II. EXPERIMENT

Experiments on measuring the energy dependence of the total cross sections for the $^{11}\mathrm{Li} + {}^{28}\mathrm{Si}$ reaction were carried out by the transmission method using the CsI(Tl) $\gamma$ spectrometer. The experimental setup and the method for measuring total reaction cross sections by the detection of prompt $n, \gamma$ radiation are described in Ref. [3]. The experiment was carried out at the accelerator U-400M of the Laboratory of Nuclear Reactions, JINR, on the channel of the achromatic fragment separator ACCULINNA [9]. The primary $^{15}$N beam with energy 49.7$A$ MeV was focused on the producing $^{9}$Be target. The secondary beam of fragmentation reaction products was formed and purified by the magnetic system of the fragment separator. At the exit of the last dipole magnet of the separator, the beam entered the straight section of the ion conductor, where the system for measuring the time of flight $T_{\mathrm{TOF}}$ consisting of two scintillation detectors $\Delta E_{\mathrm{TOF1}}$, $\Delta E_{\mathrm{TOF2}}$ was located. Polyethylene plates were installed behind the detector $\Delta E_{\mathrm{TOF2}}$ to reduce the energy of the beam particles. The scheme of the setup is shown in Fig. 1.

The beam was focused on a position-sensitive two-layer strip $\Delta E$ Si detector with a thickness of 300 $\mu$m (detector 16X:16Y; see Fig. 1) located in the focal plane of the fragment separator. In the experiment, this detector was used for preliminary tuning of the beam parameters (intensity, profile, as well as isotopic composition).

The scintillation detectors AC1 and AC2 were installed in such a way that the trajectories of particles passed through the sensitive region of the target detector $\Delta E_{\mathrm{T}}$ (natural Si, 243-$\mu$m thick) and exit window 8 without touching their holders. The $\Delta E_0$ Si detector (380-$\mu$m thick) was used to generate the start signal for the information acquisition system for each event of entering of the beam particles into the $\Delta E_0$ detector as well as for subsequent offline identification of the beam particles by their ionization losses $\Delta E_0$ and time of flight $T_{\mathrm{TOF}}$. The resulting time resolution was ≈140 ps.

The target was located in the reaction chamber which was a thin-walled vacuum cylinder of stainless steel. On the outside, the cylinder was surrounded by the gamma spectrometer of six CsI(Tl) scintillators [see Fig. 1(a)] which were prisms with the base in the form of a regular hexagon. From the end, each scintillator was optically connected to the photomultiplier (PMT) and surrounded on the outside by a reflective coating consisting of three layers of Cd, Pb, and Cu plates (each 1-mm thick) for protection from the background gamma quanta. Other detectors were located outside the sensitive zone of the $\gamma$ spectrometer, which provided a minimum level of background triggering for the $\gamma$ detectors. The spectrometer with the reaction chamber was located inside a lead cube with a wall thickness of 5 cm, the outer sides of which were covered by plates of 10-cm-thick boron-containing polyethylene.

The target was installed in the center of the sensitive zone of the spectrometer, so that the solid angle covered by the CsI(Tl) detectors was $\Omega = 4\pi\eta_0$, where $\eta_0 \approx \cos\theta_{\mathrm{min}}$, $\theta_{\mathrm{min}}$ is the minimum angle between the axis of the setup and the direction of emission of a $\gamma$ quantum or a neutron from the center of the target with the entry into the volume of scintillators CsI(Tl). For the setup shown in Fig. 1, $\theta_{\mathrm{min}} \approx 30^\circ$, which, under the condition of isotropic emission of $\gamma$ quanta and neutrons, yields the geometric efficiency of their detection $\eta_0 \approx 0.85$. The emission of neutrons in a nuclear reaction is, in general, anisotropic. To take into account anisotropy of neutron emission in a nucleus-nucleus collision and others factors, one may introduce the correction $\eta$. With the relative yield of neutrons exceeding the isotropic one in the angular range $\theta_{\mathrm{min}} \leqslant \theta \leqslant \pi - \theta_{\mathrm{min}}$, the resulting detection efficiency with the correction will be lower than the geometric efficiency, $\eta < \eta_0$. In the experiments with the target, neutrons and $\gamma$ quanta in narrow forward and backward solid angles, the sum of which was $(1 - \eta_0)4\pi$, were not detected by the spectrometer. The measurement result is the lower boundary $\tilde{\sigma}_{\mathrm{R}}$ of the total reaction cross section $\sigma_{\mathrm{R}}$ and $\eta = \tilde{\sigma}_{\mathrm{R}}/\sigma_{\mathrm{R}}$. In the collision $^{11}\mathrm{Li} + {}^{28}\mathrm{Si}$, weakly bound neutrons, after separation from the $^{11}$Li nucleus, fly with a somewhat high probability at small angles relative to the direction of the initial movement of the projectile nucleus [6]. Therefore, in this case, it is possible that the actual detection efficiency is reduced in comparison with the geometric one. To estimate the correction from neutron emission anisotropy $\eta = \tilde{\sigma}_{\mathrm{R}}/\sigma_{\mathrm{R}}$, the lower boundaries $\tilde{\sigma}_{\mathrm{R}}$ of the total reaction cross sections for the $^{9}$Li and $^{6}$He nuclei with the values of the external neutron separation energy 4.06 MeV and 1.87 MeV (0.98 MeV for two neutrons) [10,11], respectively, were measured at the same facility and compared with the values of the total reaction cross sections $\sigma_{\mathrm{R}}$ obtained in a number of other studies.

Each measurement session for a certain energy of the beam was conducted both with the target and without the target. The irradiation time was chosen in such a way that the number

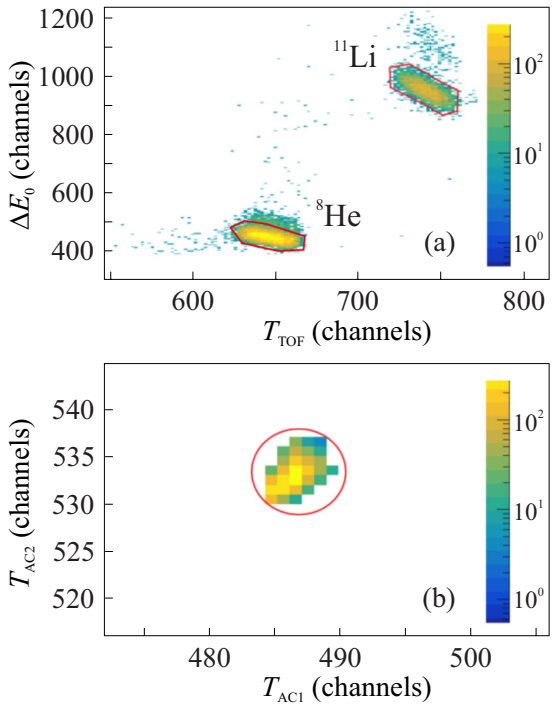


FIG. 2. (a) Two-dimensional spectrum $\Delta E_0$ $T_{\rm TOF}$ used for identification of secondary beam particles consisting of $^{8}$He and $^{11}$Li; the ionization losses of particles in the $\Delta E_0$ detector are along the ordinate axis; the time of flight of the beam particles at the distance of the time-of-flight base $L_{\rm TOF} = 8.5$ m is along the abscissa. (b) The two-dimensional spectrum $T_{\rm AC1}$ $T_{\rm AC2}$ used to select the events of $^{8}$He and $^{11}$Li particles incident on the central spot of the target. The times $T_{\rm AC1}$ and $T_{\rm AC2}$ of arrival of the signals from the detectors AC1 and AC2 relative to the start time from the $\Delta E_0$ detector are plotted along the abscissa and the ordinate axes, respectively. Events marked by points inside the contours on the spectra $\Delta E_0$ $T_{\rm TOF}$ and $T_{\rm AC1}$ $T_{\rm AC2}$ form a set of events corresponding the beam particles incident on the central spot of the target.

of events in both cases was approximately the same. The experimental information from all the detectors was recorded on a storage disk for subsequent offline analysis of each event of flight of a beam particle through the start $\Delta E_0$ detector, regardless of the reaction in the $\Delta E_{\rm T}$ detector. To reduce the effect of possible superposition of pulses in $\Delta E_0$ and $\Delta E_{\rm T}$ detectors, the beam intensity was limited to $10^3$ s$^{-1}$. The beam energy was varied without significant loss of intensity by the magnetic system of the fragment separator in the range $20A$–$30A$ MeV and by polyethylene plates in the range $7A$–$20A$ MeV.

The two-dimensional spectrum $\Delta E_0$ $T_{\rm TOF}$ for identification of secondary beam particles is shown in Fig. 2(a). It can be seen from the identification matrix that the isotopes $^{8}$He and $^{11}$Li of the beam particles form well separated regions, which makes it possible to reliably select a certain group of particles for subsequent offline analysis. Detectors AC1, AC2 were used as active collimators and served for selecting the events of flight of beam particles in a given solid angle with the axis at the center of the target. Figure 2(b) shows the two-dimensional correlation spectrum $T_{\rm AC1}$ $T_{\rm AC2}$. Points in the central region of the two-dimensional spectrum indicate events corresponding to the signals from both detectors AC1, AC2 in a narrow time interval, i.e., the events of flight of beam particles through both detectors.

The number $\Delta I$ of reaction events from the number $I_0$ of pre-selected events was determined using the logical conditions for registering a $\gamma$ quantum or a neutron at least in one of the six detectors of the spectrometer. The condition for registering a $\gamma$ quantum or a neutron in each CsI(Tl) detector was described by a contour on the two-dimensional amplitude-time $E_{\rm Cs}$ $T_{\rm Cs}$ spectrum.

The uncertainties $\delta_E$ associated with the spread of the beam energy before the target were determined from the analysis of one-dimensional spectra $\Delta E_0$ and $T_{\rm TOF}$. The energy losses $E_1$ of the projectile nuclei at the exit from the target were calculated using the LISE++ program [12]. The spread of energy losses in the target was determined by the expression $\Delta_E = (E_0 - E_1)/2 \gg \delta_E$. The value of the cross section was attributed to the value of energy $E_0 - \Delta_E$.

The beam transmission method used in the experiment consisted in measuring the flux $I_0$ of particles incident on the target with respect to its part $\Delta I$ corresponding to inelastic reaction channels. The quantity $\Delta I$ is equal to the difference in the flux $I_0$ of particles incident on the target and the flux $I$ of particles passing through the target without interaction,

$$\Delta I = I_0[1 - \exp(-n\sigma_{\rm R})], \tag{1}$$

where $n$ is the number of target nuclei per unit area. In experiments with thin targets, when the condition $\Delta I = I_0 - I \ll I_0$ is satisfied, formula (1) may be reduced to the form,

$$\sigma_{\rm R} = \frac{\Delta I}{I_0 n}. \tag{2}$$

Ideally, a decrease $\Delta I$ of the particle flux $I_0$ corresponding to inelastic reaction channels can be measured by a $4\pi$ detector covering the entire solid angle around the target. In practice, the solid angle is smaller, and a quantity $\Delta\tilde{I} = \eta\Delta I$ is measured, where $\eta$ is the correction from neutron emission anisotropy. The value $\Delta\tilde{I}$ was determined taking into account the detection efficiency of $\gamma$ quanta and neutrons by detectors minus the background.

## III. RESPONSE FUNCTION OF GAMMA SPECTROMETER

To determine the detection efficiency $P$ of gamma quanta with different multiplicities $M$ by the CsI(Tl) spectrometer (spectrometer response), measurements were performed with a $^{60}$Co calibration source installed instead of the target and an additional scintillation detector $CeBr_3$ of dimensions $51 \times 51 \times 51$ mm$^3$ positioned at the beam axis at a distance of 10 cm from the $^{60}$Co source.

After beta decay of $^{60}$Co, the excited state $4^+$ of $^{60}$Ni is formed. With probability 0.988, it emits the first gamma quantum with energy $E_{\gamma,1} = 1173$ keV in the transition from the $4^+$ state to the $2^+$ state and the second gamma quantum with energy $E_{\gamma,2} = 1332$ keV in the transition to the ground state $0^+$. The lifetime of $2^+$ state is about 0.7 ps.

A set $G_1$ of events of registration of particles with energy release $1173 \pm 10$ keV in the $CeBr_3$ scintillation detector

was recorded. These events, in the overwhelming number of cases, correspond to the emission of gamma quantum with energy $E_{\gamma,1}$ from $^{60}$Ni. The exceptions are background events that form a pedestal in the energy spectrum under the total absorption peak. The total number of events in the set $G_1$ is denoted by $n_1$. According to the $^{60}$Co decay scheme, these events should correspond to the emission from the source of the second gamma quantum with energy $E_{\gamma,2}$. Taking into account averaging over the angles of emission of the first gamma quantum entering the $CeBr_3$ detector, in the first approximation, the emission of the second gamma quantum can be considered isotropic. Events from the set $G_1$ correspond to the processes of isotropic emission of a single gamma quantum with energy $E_{\gamma,2}$ from the position of the target. The experimental detection efficiency $P$ of gamma radiation with energy $E_{\gamma,2}$ and multiplicity $M = 1$ by the CsI(Tl) spectrometer was determined as

$$P(1) = \frac{1}{n_1}\sum_{k=1}^{M} N_k^{(1)}, \tag{3}$$

where $N_k^{(1)}$ is the number of events from $G_1$ in which $k$ detectors of the spectrometer were triggered with energy release above the threshold (150 keV).

By successive combination of events from the set $G_1$ in pairs 1–2, 3–4, 5–6, etc., a set $G_2$ of events was obtained corresponding to the emission of two gamma quanta with energy $E_{\gamma,2}$. The total number of such events is denoted as $n_2 = n_1/2$. This way the emission of two gamma quanta with energy $E_{\gamma,2}$ was simulated. The experimental detection efficiency of gamma radiation with energy $E_{\gamma,2}$ and multiplicity $M = 2$ by the CsI(Tl) spectrometer was determined as

$$P(2) = \frac{1}{n_2}\sum_{k=1}^{M} N_k^{(2)}, \tag{4}$$

where $N_k^{(2)}$ is the number of events from $G_2$ in which $k$ detectors of the spectrometer were triggered with energy release above the threshold.

In the general case, a set $G_M$ of events was formed in which isotropic emission of $M$ gamma quanta with energy $E_{\gamma,2}$ occurred and the number $n_M$ of such events and the number of events $N_k^{(M)}$ from the set $G_M$ in which triggering of at least one of the CsI(Tl) detectors with energy release above the threshold was recorded. Combining events in groups of $M$, we modeled the process of emission of $M$ gamma quanta. The experimental detection efficiency of gamma radiation with energy $E_{\gamma,2}$ and multiplicity $M$ by the CsI(Tl) spectrometer was determined as

$$P(M) = \frac{1}{n_M}\sum_{k=1}^{M} N_k^{(M)}, \tag{5}$$

where we restricted ourselves to $M \leqslant 5$ (for explanation, see the last paragraph of Sec. IV).

The obtained dependence of the experimental detection efficiency of the spectrometer on the multiplicity $M \leqslant 5$ of gamma radiation with an energy of $E_{\gamma,2} = 1332$ keV is shown in Fig. 3(a). It is seen that with increasing multiplicity,

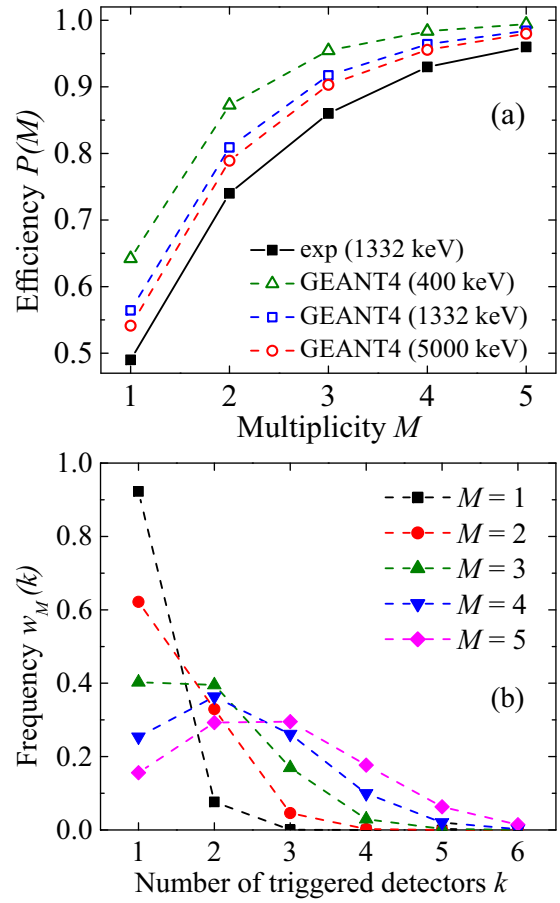


FIG. 3. (a) Detection efficiency of a group of $M$ photons by the spectrometer (spectrometer response). Experimental results for gamma energy 1332 keV (filled squares) and GEANT4 [13] calculations for gamma energies 400 keV (triangles), 1332 keV (empty squares), and 5000 keV (circles). (b) The relative frequencies $w_M(k)$ of the number of triggered spectrometer detectors in the registration of $M$ photons.

$P(M) \to 1$; for multiplicity $M \geqslant 5$, the efficiency value is $\geqslant$0.96.

To check the correctness of the obtained detection efficiency, a computer simulation of the isotropic emission of gamma quanta of various multiplicity with energies of 400 keV, 1332 keV, and 5000 keV was performed using the GEANT4 code [13]. The results are also presented in Fig. 3(a). It can be seen that the obtained experimental detection efficiency for energy 1332 keV is close to the result obtained using the GEANT4 simulation. The experimental efficiency obtained with $^{60}$Co is slightly lower than that obtained with GEANT4 because of the presence of a pedestal under the total absorption peak of the 1173-keV line in the energy spectrum of the $CeBr_3$ detector. Events corresponding to the pedestal correspond to the registration of background gamma quanta by the $CeBr_3$ detector, which leads to an overestimation of the denominators in formulas (3)–(5). GEANT4 calculations performed for a wide energy range from 400 keV to 5 MeV showed that the dependence of the efficiency on the energy of gamma quanta is weak, which is an additional justification

TABLE I. The numbers $N'_k$ of triggering of $k$ detectors, the coefficients $\beta_k$ and their uncertainties $\delta\beta_k$ for several energies $E$ and fluxes $I_0$ of the $^{9,11}$Li and $^6$He nuclei with exposures without the target.

| Nucleus | $E$ ($A$ MeV) | $I_0$ | $N'_1$ | $N'_2$ | $N'_3$ | $N'_4$ | $N'_5$ |
|---|---|---|---|---|---|---|---|
| $^{11}$Li | 7.8 | 24 840 | 26 | 10 | 4 | 1 | 0 |
| | 11.2 | 74 936 | 45 | 20 | 6 | 2 | 0 |
| | 14.9 | 74 155 | 55 | 16 | 9 | 3 | 1 |
| | 22.9 | 103 239 | 81 | 30 | 14 | 2 | 1 |
| | 26.3 | 139 013 | 99 | 47 | 17 | 7 | 2 |
| | | $\beta_k$ | $7.24 \times 10^{-4}$ | $3.01 \times 10^{-4}$ | $1.2 \times 10^{-4}$ | $3.78 \times 10^{-5}$ | $1.09 \times 10^{-5}$ |
| | | $\delta\beta_k$ | $8.94 \times 10^{-5}$ | $5.91 \times 10^{-5}$ | $2.44 \times 10^{-5}$ | $1.79 \times 10^{-5}$ | $5.7 \times 10^{-6}$ |
| $^9$Li | 36.2 | 283 729 | 227 | 41 | 17 | 6 | 0 |
| | | $\beta_k$ | $8 \times 10^{-4}$ | $1.4 \times 10^{-4}$ | $6.0 \times 10^{-5}$ | $2.1 \times 10^{-5}$ | 0 |
| $^6$He | 39.1 | 213 213 | 191 | 53 | 19 | 6 | 3 |
| | | $\beta_k$ | $9 \times 10^{-4}$ | $2.5 \times 10^{-4}$ | $8.9 \times 10^{-5}$ | $2.8 \times 10^{-5}$ | $1.4 \times 10^{-5}$ |

for the applicability of the obtained experimental detection efficiency when analyzing the data.

The relative frequencies $w_M(k)$ of the number of triggered spectrometer detectors in the registration of $M$ photons were determined as

$$w_M(k) = \frac{N_k^{(M)}}{n_M P(M)}. \tag{6}$$

The results are shown in Fig. 3(b). The probability of the number $k$ of triggered $\gamma$-spectrometer detectors in the registration of $M$ photons is equal to $P(M)w_M(k)$.

## IV. ANALYSIS OF RESULTS OF MEASUREMENTS

Sessions without the target were used to measure the background. Let $N'_k$ be the number of triggering of $k$ detectors for measurements without the target. The relationship between the number $N'_k$ and the flux $I_0$ can be approximated by a linear dependence,

$$N'_k = N'_{0k} + \beta_k I_0. \tag{7}$$

The values of the coefficients $\beta_k$ and their uncertainties $\delta\beta_k$ can be determined using linear regression. In practice, the values of the parameters $N'_{0k}$ are small in magnitude, so we will use a simpler expression,

$$N'_k = \beta_k I_0, \tag{8}$$

with the coefficients $\beta_k$ found by the least squares method from the results of $m$ measurements,

$$\beta_k = \frac{\sum_{j=1}^{m} I_{0j} N'_{kj}}{\sum_{j=1}^{m} I_{0j}^2}. \tag{9}$$

The numbers $N'_k$ of triggering of $k$ detectors, the coefficients $\beta_k$, and their uncertainties $\delta\beta_k$ for several energies $E$ and fluxes $I_0$ of the $^{9,11}$Li and $^6$He nuclei with exposures without the target are given in Table I.

The result of measuring the reaction cross section was determined taking into account the numbers of triggering of detectors in the following order. Let $M$ photons and/or neutrons be emitted in the reaction with a probability $\Gamma(M)$. Then the probability of registration, after the reaction, of $k$ photons and/or neutrons (with triggering of $k$ detectors) is equal to

$$\sum_{M=1}^{5} \Gamma(M)P(M)w_M(k). \tag{10}$$

For the total number of interactions $\Delta I = I_0\sigma_R n$, the estimated number of their registrations with triggering of $k$ detectors will be

$$\Delta\tilde{I} \sum_{M=1}^{5} \Gamma(M)P(M)w_M(k) = I_0\eta\sigma_R n \sum_{M=1}^{5} \Gamma(M)P(M)w_M(k). \tag{11}$$

Denote $N_k$ the number of registered events with the triggering of $k$ detectors. From the condition of equality of the number of registered events $N_k - N'_k = N_k - \beta_k I_0$ to their calculated value,

$$N_k - \beta_k I_0 = I_0\eta\sigma_R n \sum_{M=1}^{5} \Gamma(M)P(M)w_M(k) = I_0\eta n \sum_{M=1}^{5} \sigma_{RM} P(M)w_M(k), \tag{12}$$

follows a system of linear equations,

$$\sum_{M=1}^{5} \tilde{\sigma}_{RM} P(M)w_M(k) - \frac{N_k - \beta_k I_0}{I_0 n} = 0, \tag{13}$$

for the unknowns $\tilde{\sigma}_{RM} = \eta\sigma_{RM} = \eta\sigma_R\Gamma(M)$.

Because the coefficients of system (13) are determined with uncertainties, its exact solution may yield nonphysical values $\tilde{\sigma}_{RM} < 0$. Therefore, it is more correct to find these values from the condition that the sum of the squares of the left-hand sides is minimum,

$$F(\tilde{\sigma}_{R1}, \ldots, \tilde{\sigma}_{R5}) = \sum_{k=1}^{5} \left[ \sum_{M=1}^{5} \tilde{\sigma}_{RM} P(M)w_M(k) - \frac{N_{\gamma k} - \beta_k I_0}{I_0 n} \right]^2, \tag{14}$$

under the constraint $\tilde{\sigma}_{\mathrm{R}\,M} \geqslant 0$. The total reaction cross section can be found as

$$\sigma_{\mathrm{R}} = \frac{\tilde{\sigma}_{\mathrm{R}}}{\eta}, \tag{15}$$

$$\tilde{\sigma}_{\mathrm{R}} = \sum_{M=1}^{5} \tilde{\sigma}_{\mathrm{R}\,M}. \tag{16}$$

The uncertainty in $\Delta\tilde{\sigma}_{\mathrm{R}}$ resulting from the uncertainty $\delta\beta_k$ of the coefficients $\beta_k$ was calculated by the formula,

$$\Delta\tilde{\sigma}_{\mathrm{R}} = |\tilde{\sigma}_{\mathrm{R}}^{(+)} - \tilde{\sigma}_{\mathrm{R}}^{(-)}|/2, \tag{17}$$

where $\tilde{\sigma}_{\mathrm{R}}^{(+)}$ and $\tilde{\sigma}_{\mathrm{R}}^{(-)}$ are the values for the set of parameters $\beta_k + \delta\beta_k$ and $\beta_k - \delta\beta_k$, respectively. The values of the relative $\varepsilon_\sigma$ and absolute $\Delta\sigma_{\mathrm{R}}$ uncertainties were calculated by formulas,

$$\varepsilon_\sigma = \frac{\Delta\tilde{\sigma}_{\mathrm{R}}}{\tilde{\sigma}_{\mathrm{R}}} + \frac{\Delta\eta}{\eta}, \tag{18}$$

$$\Delta\sigma_{\mathrm{R}} = \sigma_{\mathrm{R}}\varepsilon_\sigma. \tag{19}$$

The correction $\eta$ can be estimated by comparison of the lower boundaries of the total cross sections for the $^{9}\mathrm{Li} + {}^{28}\mathrm{Si}$, $^{6}\mathrm{He} + {}^{28}\mathrm{Si}$ reactions with the known data from other studies.

For the reaction $^{9}\mathrm{Li} + {}^{28}\mathrm{Si}$ [see Fig. 4(a)], the correction $\eta$ was taken to be equal to $\eta_0 = 0.85$. It makes the experimental point as close as possible to the total reaction cross section smoothed by splines without exceeding the geometric efficiency $\eta_0$. This may be an indication of isotropic emission of gamma quanta and neutrons.

Taking into account the experimental energy dependence of the total cross section for the reaction $^{6}\mathrm{He} + {}^{28}\mathrm{Si}$ smoothed by splines and uncertainties of experimental points [Fig. 4(b)], we obtained the upper and lower boundaries of the confidence interval for the total reaction cross section and an interval estimate for the correction $\eta = \langle\eta\rangle \pm \Delta\eta$, where $\langle\eta\rangle = 0.78$, $\Delta\eta = 0.04$.

The numbers $N_k$ of triggering of $k$ detectors, the lower boundaries $\tilde{\sigma}_{\mathrm{R}}$ of the total cross sections, the total cross sections $\sigma_{\mathrm{R}}$, and the correction $\eta$ for one value of energy $E$ and flux $I_0$ of the $^{6}\mathrm{He}$ and $^{9}\mathrm{Li}$ nuclei in exposures with the target are given in Table II.

The dependence of $\eta$ on the separation energy of one and two external neutrons for the $^{9}\mathrm{Li}$ and $^{6}\mathrm{He}$ nuclei is shown in Fig. 5. It can be seen that it correlates with the separation energies of external neutrons, so the extrapolation of this dependence for the binding energy of one 0.396 MeV and two 0.369 MeV [10,11] external neutrons of the $^{11}\mathrm{Li}$ nucleus makes it possible to obtain an interval estimate of the correction $\langle\eta\rangle = 0.73$, $\Delta\eta = 0.03$ for the reaction $^{11}\mathrm{Li} + {}^{28}\mathrm{Si}$. The obtained value of the correction $\eta < \eta_0$ for the reaction $^{11}\mathrm{Li} + {}^{28}\mathrm{Si}$ may be an indication of neutron emission anisotropy and breakup of the $^{11}\mathrm{Li}$ nucleus without emission of gamma quanta.

The numbers $N_k$ of triggering of $k$ detectors for different energies $E$ and fluxes $I_0$ of the $^{11}\mathrm{Li}$ nuclei in exposures with the target are given in Table III. Analysis of the results of measurements with the beams of the $^{11}\mathrm{Li}$ nuclei using the value of the correction $\eta = 0.73$ yielded the values of the total

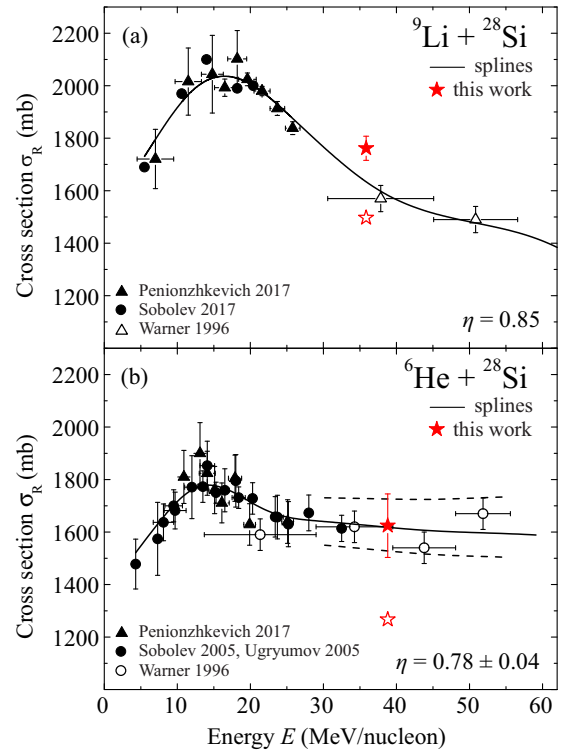


FIG. 4. Experimental (symbols) and smoothed by splines (curves) energy dependence of the total cross sections for the reactions $^{9}\mathrm{Li} + {}^{28}\mathrm{Si}$ (a): filled circles (Sobolev 2017 [3]), filled triangles (Penionzhkevich 2017 [2]), empty triangles (Warner 1996 [5]); (b) $^{6}\mathrm{He} + {}^{28}\mathrm{Si}$: empty circles (Warner 1996 [5]), filled triangles (Penionzhkevich 2017 [2]), filled circles (Sobolev 2005 [14], Ugryumov 2005 [15]); the results of this work: empty stars are the lower boundaries of the total reaction cross sections $\tilde{\sigma}_{\mathrm{R}}$, filled stars are the total reaction cross sections $\sigma_{\mathrm{R}}$ for correction $\eta = \eta_0 = 0.85$ (a) and $\eta = 0.78 \pm 0.04$ (b). The dashed lines (b) are the upper and lower boundaries of the confidence interval for the total reaction cross section.

TABLE II. The total reaction cross sections $\sigma_{\mathrm{R}}$ and the corrections for one value of energy $E$ and flux $I_0$ of the $^{6}\mathrm{He}$ and $^{9}\mathrm{Li}$ nuclei in exposures with the target.

| Nucleus | $E$ ($A$ MeV) | $I_0$ | $N_1$ | $N_2$ | $N_3$ | $N_4$ | $N_5$ | $\tilde{\sigma}_{\mathrm{R}}$ (mb) | $\sigma_{\mathrm{R}}$ (mb) | $\eta$ |
|---|---|---|---|---|---|---|---|---|---|---|
| $^{6}\mathrm{He}$ | 38.8 ± 0.3 | 244 884 | 315 | 122 | 52 | 16 | 6 | 1267 | 1624 ± 121 | 0.78 ± 0.04 |
| $^{9}\mathrm{Li}$ | 35.9 ± 0.3 | 300 366 | 399 | 143 | 76 | 37 | 14 | 1497 | 1761 ± 46 | 0.85 |

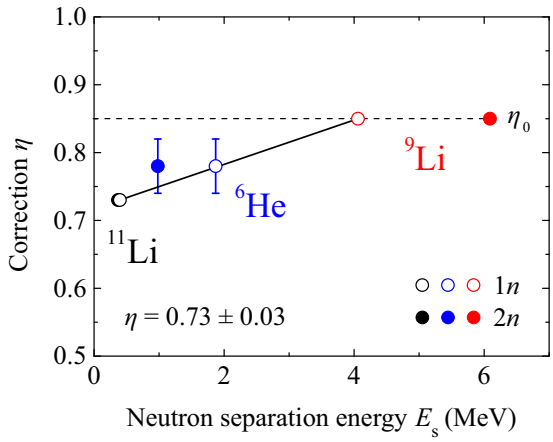


FIG. 5. The dependence of the correction $\eta$ on the separation energy of one (empty circles) and two (filled circles) external neutrons for the $^9$Li and $^6$He nuclei. Solid line is the result of linear interpolation.

reaction cross section given in Table IV and shown in Fig. 6. For comparison, Fig. 6 also shows data for the $^{11}\mathrm{Li} + {}^{28}\mathrm{Si}$ reaction obtained in other studies and data for the $^9\mathrm{Li} + {}^{28}\mathrm{Si}$ reaction.

It is evident that the data obtained are in agreement with the results of Refs. [5,16,17] and also cover the previously unexplored range of low energies. The cross section for the $^{11}\mathrm{Li} + {}^{28}\mathrm{Si}$ reaction was measured in the energy range $7A$–$25A$ MeV where a maximum is observed reaching a value of about 3 barns, which is much larger than the values of the cross sections for the reactions $^6\mathrm{He} + {}^{28}\mathrm{Si}$ and $^9\mathrm{Li} + {}^{28}\mathrm{Si}$ [2].

Because the experimental results for the reactions $^6$He, $^9$Li, $^{11}\mathrm{Li} + {}^{28}\mathrm{Si}$ given in Tables I–III reveal a sharp decrease of the numbers of triggering of $k$ detectors with the increase of $k$ both in exposures with the target $N_k$ and without the target $N'_k$, we restricted ourselves to $M \leqslant 5$.

## V. MICROSCOPIC DESCRIPTION OF NEUTRONS IN $^{11}$Li NUCLEI

It is well known that the $^7$Li, $^9$Li, $^{11}$Li nuclei are deformed, the experimental values of the quadrupole deformation parameter $\beta_2$ are from –0.9 to –1.5 for $^7$Li, from –0.6 to –0.8 for $^9$Li, –0.6 for $^{11}$Li [11,18]. Calculations in the shell model of the deformed nucleus by the method of Ref. [19] provided the

TABLE III. The numbers $N_k$ of triggering of $k$ detectors for different energies $E$ and fluxes $I_0$ of the $^{11}$Li nuclei in exposures with the target.

| $E$ ($A$ MeV) | $I_0$ | $N_1$ | $N_2$ | $N_3$ | $N_4$ | $N_5$ |
|---|---|---|---|---|---|---|
| 6.9 ± 1.0 | 21 149 | 23 | 18 | 16 | 3 | 1 |
| 10.5 ± 0.7 | 86 525 | 122 | 87 | 53 | 21 | 7 |
| 14.3 ± 0.6 | 72 927 | 107 | 62 | 33 | 19 | 6 |
| 22.5 ± 0.4 | 148 057 | 201 | 140 | 66 | 44 | 10 |
| 25.4 ± 0.4 | 135 552 | 180 | 120 | 66 | 21 | 9 |

TABLE IV. Experimental values of the total cross sections for the reaction $^{11}\mathrm{Li} + {}^{28}\mathrm{Si}$ as a function of energy $E$.

| $E$ ($A$ MeV) | $\sigma_R$ (mb) |
|---|---|
| 6.9 ± 1.0 | 2144 ± 296 |
| 10.5 ± 0.7 | 2849 ± 408 |
| 14.3 ± 0.6 | 2695 ± 391 |
| 22.5 ± 0.4 | 2520 ± 384 |
| 25.4 ± 0.4 | 2297 ± 386 |

energies of the upper occupied levels of the nuclei $^7$Li and $^9$Li, approximately equal to the experimental values of the neutron separation energy taken with the opposite sign. The obtained neutron-level diagrams are shown in Figs. 7(a)–7(c). The used values of the quadrupole deformation parameters $\beta_2$, the parameters of the Woods-Saxon potential,

$$U(r, \cos\theta) = -U_0(1 + \exp\{[r - R_U f_\beta(\cos\theta)]/a_U\})^{-1}, \quad (20)$$

with the expression for $f_\beta(\cos\theta)$ from Ref. [20] and the dimensionless spin-orbit strength $\lambda$ [21] for neutrons in the $^7$Li, $^9$Li, $^{11}$Li nuclei are given in Table V.

Two neutrons and two protons at deep lower levels corresponding to the level $1s_{1/2}$ of the spherical nucleus with the projection of the total angular momentum on the axis of symmetry of the nucleus $|m_j| = 1/2$ belong to a nuclear core similar to an alpha cluster. The two external neutrons of the $^7$Li nucleus on the sublevel with the projection of the total angular momentum on the axis of symmetry of the nucleus $|m_j| = 3/2$ corresponding to the level $1p_{3/2}$ of the spherical nucleus can be considered quite strongly bound to the nuclear core: their separation energy is 7.25 MeV. In the $^9$Li nucleus, the neutron separation energy for this sublevel is noticeably

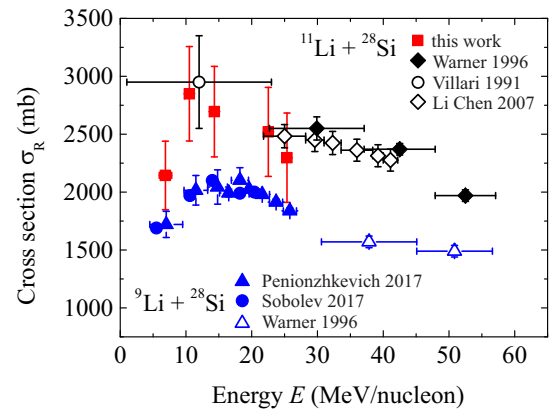


FIG. 6. Experimental energy dependence of the total cross sections for the reaction $^{11}\mathrm{Li} + {}^{28}\mathrm{Si}$: filled (red) squares are the results of this work. The remaining data for $^{11}$Li: filled diamonds (Warner 1996 [5]), empty circle (Villari 1991 [16]), and empty diamonds (Li Chen 2007 [17]). Data for $^9\mathrm{Li} + {}^{28}\mathrm{Si}$: filled circles (Sobolev 2017 [3]), filled triangles (Penionzhkevich 2017 [2]), and empty triangles (Warner 1996 [5]).

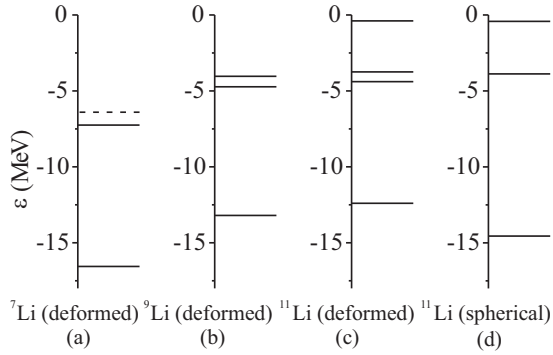


FIG. 7. Schemes of neutron levels for the nuclei $^{7}$Li (a), $^{9}$Li (b), and $^{11}$Li (c) in the shell model of the deformed nucleus and in the shell model of the spherical nucleus $^{11}$Li (d).

smaller, and for the higher-lying sublevel with $|m_j| = 1/2$ the separation energy is 4.06 MeV. Thus, for the four external neutrons of the $^{9}$Li nucleus, the bond with the alpha-cluster core is weakened. In collisions with heavy nuclei, the probability density distribution for these neutrons can change more significantly than for the two external neutrons of the $^{7}$Li nucleus.

The level scheme for the neutrons of the $^{11}$Li nucleus with the quadrupole deformation parameter $\beta_2 = -0.6$ is shown in Fig. 7(c). Because the $^{10}$Li nucleus is unbound, two external neutrons in the $^{11}$Li nucleus are bound only by pairing forces. In the deformed nucleus $^{11}$Li, the energies of the sublevels with $|m_j| = 3/2$ and $|m_j| = 1/2$ corresponding to the level $1p_{3/2}$ of the spherical nucleus, turn out to be close. This makes it possible, with sufficient accuracy, to use the spherical shell model for the $^{11}$Li nucleus with three filled neutron shells: $1s_{1/2}$ (in the alpha-cluster core), $1p_{3/2}$ (the first inner shell), and $1p_{1/2}$ (external halo shell). Thus, the Woods-Saxon potential had the form,

$$U(r) = -U_0\{1 + \exp[(r - R_U)/a_U]\}^{-1}, \quad (21)$$

with the parameters given in Table V.

The spherical shell model is poorly applicable for description of the nucleons in the target nucleus $^{28}$Si, because the proton probability density distribution in it, as a result of the states with the nonzero orbital angular momentum $1p^4_{3/2}$, $1p^2_{1/2}$, $1d^6_{5/2}$, is essentially inhomogeneous and does not agree with the experimental charge distribution [2,11]. The result of averaging over all possible orientations of the symmetry axis of the charge distribution in a nonspherical nucleus with a negative quadrupole deformation parameter is close to the experimental charge distribution [2,11,18]. To describe the influence of the target nucleus on the external neutrons of the projectile nucleus at the initial stage of penetration of the projectile neutrons into the target nucleus, we can use the result of averaging of the potential of the deformed nucleus over the isotropic distribution of the orientation of the symmetry axis. The values of the parameters of the potential for neutrons in the $^{28}$Si nucleus are given in Table V.

TABLE V. Values of the parameters of the shell model.

| Nucleus | $\beta_2$ | $U_0$ (MeV) | $r_0$ (fm) | $R_U = r_0 A^{1/3}$ (fm) | $a_U$ (fm) | $\lambda$ |
|---|---|---|---|---|---|---|
| $^{7}$Li | −1 | 38.7 | 1.3 | 2.49 | 0.95 | 21 |
| $^{9}$Li | −0.7 | 32 | 1.3 | 2.70 | 0.95 | 21 |
| $^{11}$Li | −0.6 | 29.4 | 1.3 | 2.89 | 0.95 | 21 |
| $^{11}$Li | 0 | 33.3 | 1.25 | 2.78 | 0.65 | 35 |
| $^{28}$Si | 0 | 54 | 1.17 | 3.54 | 0.8 | 30 |

## VI. CALCULATION OF TOTAL REACTION CROSS SECTIONS IN TIME-DEPENDENT APPROACH

As in Refs. [4,5], we consider two main groups of reaction channels, those that are the consequence of the interaction of the $^{9}$Li-like core of the $^{11}$Li nucleus with the $^{28}$Si nucleus and the consequence of neutron loss from the outer shell $1p^2_{1/2}$ of the $^{11}$Li nucleus. The loss of one neutron (with some probability) leads to a subsequent loss of the second neutron by the unbound $^{10}$Li nucleus. The independent probabilities $P_{\rm core}$ of the reaction resulting from the interaction with the $^{9}$Li-like core of the $^{11}$Li nucleus and $P_{\rm loss}$ of the neutron loss from the outer shell can be determined as functions of energy $E$ and the impact parameter $b$ in the semiclassical model: $P_{\rm core}(b, E)$, $P_{\rm loss}(b, E)$. The total reaction cross section $\sigma_{\rm R}$ can be expressed in terms of these probabilities. The probability of absence of the reaction involving the core is equal to $1 - P_{\rm core}(b, E)$, the probability of absence of loss of at least one neutron is $[1 - P_{\rm loss}(b, E)]^2$, and the probability of none of these events is equal to

$$[1 - P_{\rm core}(b, E)][1 - P_{\rm loss}(b, E)]^2. \quad (22)$$

The probability of the reaction involving the core or because of the loss of a neutron from the outer shell of the $^{11}$Li nucleus is equal to

$$P_{\rm R}(b, E) = 1 - [1 - P_{\rm core}(b, E)][1 - P_{\rm loss}(b, E)]^2. \quad (23)$$

The total cross section for the $^{11}$Li + $^{28}$Si reaction in the semiclassical approach is represented by an integral over impact parameters,

$$\sigma_{\rm R} = 2\pi \int_0^\infty P_{\rm R}(b, E) b db. \quad (24)$$

The semiclassical expression for the total cross section of the reaction $^{9}$Li + $^{28}$Si,

$$\sigma_{\rm R} = 2\pi \int_0^\infty P_{\rm core}(b, E) b db, \quad (25)$$

corresponds to the sum over the orbital angular momenta in the quantum approach,

$$\sigma_{\rm R} = \frac{\pi}{k^2} \sum_{l=0}^{\infty} (2l + 1) \tilde{P}_{\rm core}(l, E), \quad (26)$$

taking into account the relation $l \sim kb$, where $k$ is the modulus of the wave vector. The calculation of the total cross section $\sigma_{\rm R}$ for the reaction $^{9}$Li + $^{28}$Si and the probability $\tilde{P}_{\rm core}(l, E)$,

$$\tilde{P}_{\rm core}(l, E) = 1 - |S_l|^2, \quad (27)$$

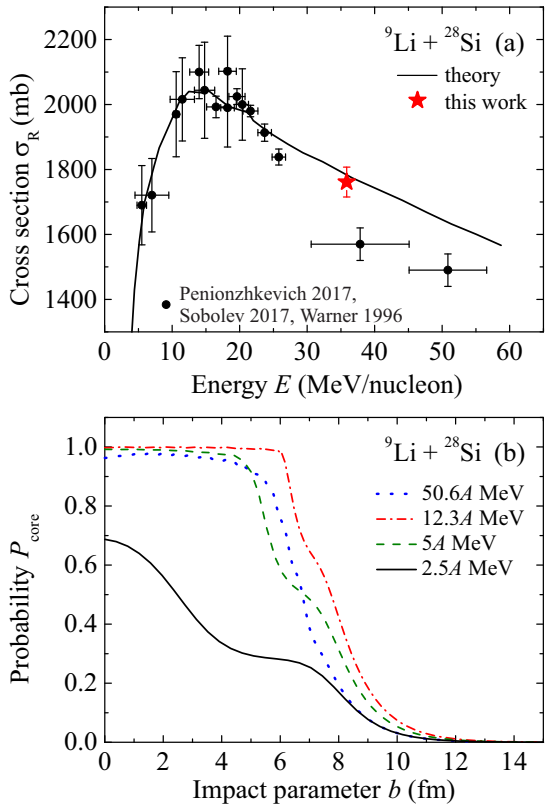


FIG. 8. (a) The total cross section for the $^9$Li + $^{28}$Si reaction. Filled circles are the experimental data from Fig. 4(a) (Sobolev 2017 [3], Penionzhkevich 2017 [2], Warner 1996 [5]); the curve is the result of calculations in the optical model with the energy-dependent optical potential [2]. (b) Probabilities $P_{\rm core}(b, E) = \tilde{P}_{\rm core}(kb, E)$ depending on the impact parameter $b$ for energies 2.5$A$ MeV (solid line), 5$A$ MeV (dashed line), 12.3$A$ MeV (dash-dotted line), and 50.6$A$ MeV (dotted line).

where $S_l$ is the diagonal element of the $S$ matrix in the optical model with the energy-dependent optical potential, was performed in Ref. [2] based on the solution of the time-dependent Schrödinger equation for external neutrons of the $^9$Li nucleus. The comparison of the results of calculations with the experimental data is shown in Fig. 8(a). The dependence of the probabilities $P_{\rm core}(b, E) = \tilde{P}_{\rm core}(kb, E)$ on $b$ is shown in Fig. 8(b). An increase in the cross section of the reaction is most noticeable in the energy range at which the relative velocity of the nuclei is close in magnitude to the average velocity of external neutrons in the investigated weakly bound nuclei [2].

For calculation of the probability $P_{\rm loss}$ of neutron loss from the outer shell, we use a time-dependent approach with a quantum description of neutrons in combination with motion of the centers of colliding nuclei along classical trajectories [19,22,23]. The two-component spinor wave function $\Psi(\mathbf{r}, t)$ of each of the two independent neutrons with the radius vector $\mathbf{r}$ and the initial state $1p_{1/2}$ was calculated by numerical solution of the time-dependent Schrödinger equation (TDSE) taking into account spin-orbit interaction [2,24,25]. On the Cartesian grid coordinates, the splitting method [26,27]

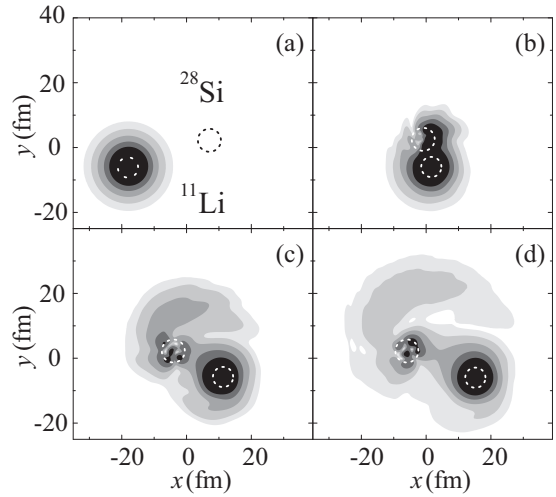


FIG. 9. An example of the evolution of the probability density for external neutrons of the $^{11}$Li nucleus in the collision with the $^{28}$Si nucleus at energy $E = 12.6A$ MeV. The location of panels (a)–(d) corresponds to time.

results in the difference scheme of the second-order accuracy. The time-dependent Schrödinger equation is solved iteratively in time with the fast complex Fourier transform [27] on a spatial grid with a plane of symmetry (the collision plane). The lattice spacing in the TDSE method is 0.15 fm, which is substantially smaller than 0.8 fm in a typical time-dependent Hartree-Fock calculation [28]. The colliding nuclei are enclosed in a box of typical dimensions $90 \times 75 \times 40$ fm$^3$. An example of the evolution of the probability density of external neutrons of the $^{11}$Li nucleus in the collision with the $^{28}$Si nucleus is shown in Fig. 9. It can be seen that, at energies $\approx 10A$ MeV, the external neutrons lost by the $^{11}$Li nucleus are transferred to the target nucleus $^{28}$Si or leave both nuclei with energy in the continuous spectrum with comparable probabilities $P_{\rm d}$ and $P_{\rm c}$, respectively.

The probabilities $P_{\rm d}(b, E)$ of neutron transfer to unoccupied bound states of the discrete spectrum in the $^{28}$Si nucleus determined in the same way as in Refs. [24,25], are shown in Fig. 10(a) as functions of the distance of the closest approach $R_{\rm min}(b, E)$ between the centers of the nuclei. The probabilities $P_{\rm c}$ of transfer to the states of the continuous spectrum can be determined by integrating the probability density outside the vicinity of the nuclei. As an estimate for $P_{\rm c}$, we can use the expression,

$$P_{\rm c} = C \max \left\{ \int_D \rho(\mathbf{r}, t) dr \right\}, \tag{28}$$

where $D$ is the spherical layer around the $^{28}$Si nucleus with boundary radii $r_1 = R_{\rm Si} + \Delta R_1$ and $r_2 = R_{\rm Si} + \Delta R_2$; $R_{\rm Si}$ is the radius of the target nucleus $^{28}$Si; $C$ is a variable (adjustable) parameter. It is assumed that the released neutrons initially appear in the layer $D$ in the form of a compact three-dimensional wave packet (see Fig. 9) and then gradually leave it when the packet spreads. The dependence of the probabilities $P_{\rm c}$ on $R_{\rm min}(b, E)$ for $C = 1$, $\Delta R_1 = 3$ fm, and $\Delta R_2 = 10$ fm is shown in Fig. 10(b).

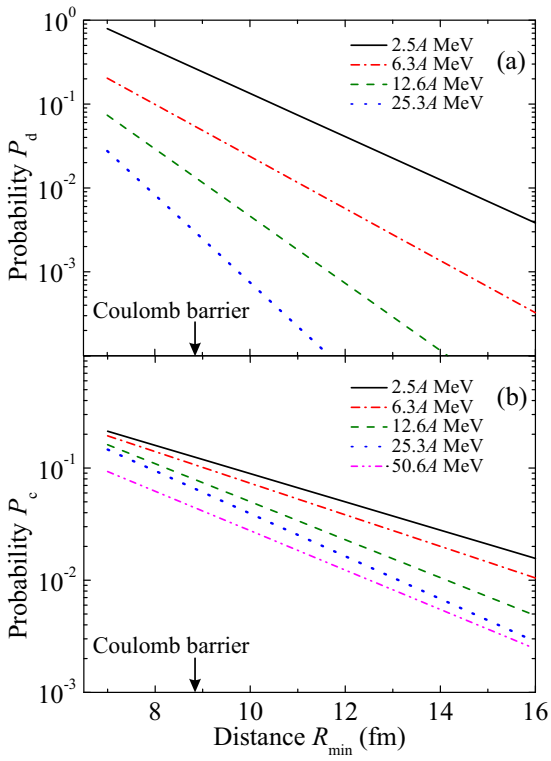


FIG. 10. The probabilities of neutron transfer to the unoccupied bound states of the discrete spectrum in the $^{28}$Si nucleus (a) and the probabilities of transfer to the states of the continuous spectrum calculated by formula (28) with $C = 1$, $\Delta R_1 = 3$ fm, and $\Delta R_2 = 10$ fm (b) for energies 2.5$A$ MeV (solid line), 6.3$A$ MeV (dash-dotted line), 12.6$A$ MeV (dashed line), 25.3$A$ MeV (dotted line), and 50.6$A$ MeV (dash-dot-dotted line). Arrows indicate the position of the Coulomb barrier.

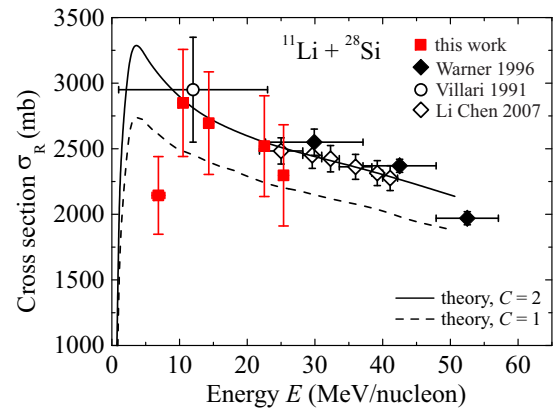


FIG. 11. The total cross section for the $^{11}$Li + $^{28}$Si reaction. Symbols are experimental data. Filled (red) squares are the results of this work, filled diamonds (Warner 1996 [5]), empty circle (Villari 1991 [16]), and empty diamonds (Li Chen 2007 [17]). Curves are the results of calculations for the values of the adjustable parameter $C = 2$ (solid curve) and $C = 1$ (dashed curve) with the probability $P_c$ of transition to the states of the continuous spectrum calculated by formula (28).

The probability $P_{loss}$ of neutron loss from the outer shell was determined by the expression,

$$P_{loss}(b, E) = \min\{P_d(b, E) + P_c(b, E), 1\}. \quad (29)$$

The results of calculations of total reaction cross section for the two values of the adjustable parameter $C = 1$ and $C = 2$ for the transition probability to the states of the continuous spectrum (28) are shown in Fig. 11. It is obvious that the value of $C = 1$ corresponds to the use of the lower boundary for the probability $P_c$, which leads to an underestimation of the calculated total reaction cross section (the dashed curve in Fig. 11). For a more realistic estimate with the value $C = 2$ (solid curve), a better agreement with the experimental data is obtained.

In the theoretical energy dependence of the total cross section, a sharp maximum is observed at energies near 5$A$ MeV. On the lower energy side, it is largely because of a sharp increase in the reaction probability $P_{core}$ of the interaction of the target nucleus with the $^9$Li-like core of the $^{11}$Li nucleus and an increase in the probability of transfer to the target nucleus of the neutron from the extended halo shell $1p^2_{1/2}$ of the $^{11}$Li nucleus. A fairly sharp decrease in the total cross section from the high-energy side at $E \approx 10A$ MeV results from the rapid decrease of the probability of neutron transfer to the target nucleus and the decrease of the reaction probability $P_{core}$ of the interaction of the target nucleus with the $^9$Li-like core of the $^{11}$Li nucleus in the region of sharp enhancement of the total cross section for the $^9$Li + $^{28}$Si reaction. The energy dependence of the probability $P_{core}$ is because of the different interaction time and the influence of the neutron layer (skin) of the inner shell $1p^4_{3/2}$, i.e., the redistribution of an appreciable part of it into the region between the surfaces of the approached nuclei (see Ref. [2]). The probability $P_c$ of transfer to the states of the continuous spectrum from the extended halo shell $1p^2_{1/2}$ changes (decreases) with increasing energy fairly smoothly. This is the reason for the enhancement of the total cross section for the reaction $^{11}$Li + $^{28}$Si in comparison with the $^9$Li + $^{28}$Si and $^7$Li + $^{28}$Si reactions (Fig. 6).

## VII. DISCUSSION

It can be seen that the results of calculation reproduce experimental data somewhat well except the point with the lowest energy. This experimental point may be underestimated because of the cold breakup contribution with neutrons not detected. Low statistics may also lead to incorrect value of the cross section. In fact, the uncertainty at this point must be larger because of low statistics, but it is difficult to estimate the contribution of statistical error in the overall error, therefore we did not do it. From the theoretical point of view, the correction from neutron emission anisotropy may depend on the collision energy because the ratio of the number of gamma quanta to the number of neutrons emitted may depend on the energy because of the different contribution of various reaction channels for different energies. To determine the dependence of the correction on energy more experimental reference points are required (here, we used only one reference point). In addition, vertical error bars for two low-energy points almost overlap. It can be concluded that more precise experimental data at this energy range is necessary.

## VIII. CONCLUSIONS

The energy dependence of the total cross section for the $^{11}$Li + $^{28}$Si reaction was measured in the beam energy range 7$A$–25$A$ MeV by the direct and model-independent transmission method. An unusual significant wide enhancement in the total cross sections for the $^{11}$Li + $^{28}$Si reaction in comparison with the $^{9}$Li + $^{28}$Si reaction was observed in the entire investigated energy range. The maximum of the measured cross section was observed at ≈10$A$ MeV. The experimental results have been compared with theoretical calculations. The total cross sections for the $^{11}$Li + $^{28}$Si reaction have been calculated based on the numerical solution of the time-dependent Schrödinger equation for the external weakly bound neutrons of the projectile nucleus $^{11}$Li. The time-dependent model proposed in the work shows that the sharp maximum in the total cross section results from the processes of neutron transfer from the external halo shell to the target nucleus and the redistribution of the appreciable part of the inner skin shell into the region between the surfaces of the approached nuclei. Such an increase in the cross section of the reaction is most noticeable in the energy range at which the relative velocity of the nuclei is close in magnitude to the average velocity of external neutrons in the investigated weakly bound nuclei. The enhancement of the cross section for the $^{11}$Li + $^{28}$Si reaction compared to those for the $^{9}$Li + $^{28}$Si and $^{7}$Li + $^{28}$Si reactions in the entire energy range (up to 50$A$ MeV) results from neutron transfer from the extended halo shell to the states of the continuous spectrum. The calculated total reaction cross sections are in good agreement with the experimental data.

## ACKNOWLEDGMENTS

The authors express their gratitude to the scientific group of the ACCULINNA setup for all possible assistance in carrying out experiments on the beams of the fragment separator. The work was supported by the Russian Science Foundation, Grant No. 17-12-01170.

[1] Yu. E. Penionzhkevich, Phys. Atom. Nucl. **74**, 1615 (2011).
[2] Yu. E. Penionzhkevich, Yu. G. Sobolev, V. V. Samarin, and M. A. Naumenko, Phys. Atom. Nucl. **80**, 928 (2017).
[3] Yu. G. Sobolev, Yu. E. Penionzhkevich, D. Aznabaev, E. V. Zemlyanaya, M. P. Ivanov, G. D. Kabdrakhimova, A. M. Kabyshev, A. G. Knyazev, A. Kugler, N. A. Lashmanov, K. V. Lukyanov, A. Maj, V. A. Maslov, K. Mendibayev, N. K. Skobelev, R. S. Slepnev, V. V. Smirnov, and D. Testov, Phys. Part. Nucl. **48**, 922 (2017).
[4] I. Tanihata, D. Hirata, T. Kobayashi, S. Shimoura, K. Sugimoto, and H. Toki, Phys. Lett. B **289**, 261 (1992).
[5] R. E. Warner, R. A. Patty, P. M. Voyles, A. Nadasen, F. D. Becchetti, J. A. Brown, H. Esbensen, A. Galonsky, J. J. Kolata, J. Kruse, M. Y. Lee, R. M. Ronningen, P. Schwandt, J. von Schwarzenberg, B. M. Sherrill, K. Subotic, J. Wang, and P. Zecher, Phys. Rev. C **54**, 1700 (1996).
[6] R. Anne, S. Arnell, R. Bimbot, H. Emling, D. Guillemaud-Mueller, P. Hansen, L. Johannsen, B. Jonson, M. Lewitowicz, S. Mattsson, A. Mueller, R. Neugart, G. Nyman, F. Pougheon, A. Richter, K. Riisager, M. Saint-Laurent, G. Schrieder, O. Sorlin, and K. Wilhelmsen, Phys. Lett. B **250**, 19 (1990).
[7] E. J. Burge, Nucl. Phys. **13**, 511 (1959).
[8] T. Gooding, Nucl. Phys. **12**, 241 (1959).
[9] A. Rodin, S. Stepantsov, D. Bogdanov, M. Golovkov, A. Fomichev, S. Sidorchuk, R. Slepnev, R. Wolski, G. Ter-Akopian, Yu. Oganessian, A. Yukhimchuk, V. Perevozchikov, Yu. Vinogradov, S. Grishechkin, A. Demin, S. Zlatoustovskiy, A. Kuryakin, S. Fil'chagin, and R. Ilkaev, Nucl. Instrum. Methods Phys. Res. Sect. B **204**, 114 (2003).
[10] M. Wang, G. Audi, A. H. Wapstra, F. Kondev, M. MacCormick, X. Xu, and B. Pfeiffer, Chin. Phys. C **36**, 1603 (2012).
[11] V. I. Zagrebaev, A. S. Denikin, A. V. Karpov, A. P. Alekseev, M. A. Naumenko, V. A. Rachkov, V. V. Samarin, and V. V. Saiko, *NRV Web Knowledge Base on Low-energy Nuclear Physics*, http://nrv.jinr.ru/.
[12] Computer code LISE++, http://lise.nscl.msu.edu/.
[13] Computer code GEANT4, http://geant4.web.cern.ch/.
[14] Yu. G. Sobolev, A. Budzanowski, E. Bialkowski, T. K. Zholdybaev, E. V. Zemlyanaya, R. Kalpakchieva, A. Kugler, I. V. Kuznetsov, A. A. Kulko, K. A. Kuterbekov, I. N. Kukhtina, V. F. Kushniruk, S. P. Lobastov, V. K. Luk'yanov, S. M. Luk'yanov, V. A. Maslov, L. Mikhailov, Yu. E. Penionzhkevich, I. Skwirczynska, N. K. Skobelev, W. H. Trzaska, and V. Yu. Ugryumov, Bull. Russ. Acad. Sci.: Phys. **69**, 1790 (2005).
[15] V. Yu. Ugryumov, I. V. Kuznetsov, E. Bialkowski, A. Kugler, K. A. Kuterbekov, I. N. Kuhtina, V. F. Kushniruk, V. G. Lyapin, V. A. Maslov, Yu. E. Penionzhkevich, Yu. G. Sobolev, W. Trzaska, G. P. Tjurin, S. V. Khlebnikov, and S. Yamaletdinov, Phys. Atom. Nucl. **68**, 16 (2005).
[16] A. C. C. Villari, W. Mittig, E. Plagnol, Y. Schutz, M. Lewitowicz, L. Bianchi, B. Fernandez, J. Gastebois, A. Gillibert, C. Stephan, L. Tassan-Got, G. Audi, W. Zhan, A. Cunsolo, A. Foti, A. Belezyorov, S. Lukyanov, and Yu. Penionzhkevich, Phys. Lett. B **268**, 345 (1991).
[17] Li Chen, Ye Yan-Lin, Zhan Wen-Long, Xiao Guo-Qing, Xu Hu-Shan, Guo Zhong-Yang, Wang Jian-Song, Sun Zhi-Yu, Li Jia-Xing, Wang Meng, Chen Zhi-Qiang, Jiang Dong-Xing, Zheng Tao, Hua Hui, Li Zhi-Huan, Li Xiang-Qing, Ge Yu-Cheng, Pang Dan-Yang, Lou Jian-Ling, Lu Fei, Fan Feng-Ying, and Lü Lin-Hui, High Energy Phys. Nucl. Phys. **31**, 1102 (2007).
[18] Centre for photonuclear experiments data, http://cdfe.sinp.msu.ru/.
[19] V. V. Samarin, Phys. Atom. Nucl. **78**, 128 (2015).
[20] V. I. Zagrebaev and V. V. Samarin, Phys. Atom. Nucl. **67**, 1462 (2004).
[21] Z. Patyk and A. Sobiczewski, Nucl. Phys. A **533**, 132 (1991).
[22] V. Samarin, EPJ Web Conf. **86**, 00040 (2015).
[23] V. I. Zagrebaev, V. V. Samarin, and W. Greiner, Phys. Rev. C **75**, 035809 (2007).
[24] M. A. Naumenko, V. V. Samarin, Yu. E. Penionzhkevich, and N. K. Skobelev, Bull. Russ. Acad. Sci.: Phys. **80**, 264 (2016).
[25] M. A. Naumenko, V. V. Samarin, Yu. E. Penionzhkevich, and N. K. Skobelev, Bull. Russ. Acad. Sci.: Phys. **81**, 710 (2017).
[26] M. E. Riley and B. Ritchie, Phys. Rev. A **59**, 3544 (1999).
[27] G. I. Marchuk, *Methods of Computational Mathematics* (Springer-Verlag, Berlin, 1981).
[28] C. Golabek and C. Simenel, Phys. Rev. Lett. **103**, 042701 (2009).